Structure of Triglyceride-Rich Human Low-Density Lipoproteins According to Cryoelectron Microscopy†

Michael B. Sherman,‡,§ Elena V. Orlova,‖ Glenn L. Decker,‡ Wah Chiu,‡ and Henry J. Pownall*,‡

Section of Atherosclerosis and Lipoprotein Research, Department of Medicine, and The Verna and Marrs McLean Department of Biochemistry and Molecular Biology, Baylor College of Medicine, Houston, Texas 77030, and School of Crystallography, Birkbeck College, University of London, London WC1E 7HX, United Kingdom

Received August 18, 2003

ABSTRACT: Low-density lipoprotein (LDL) particles from normolipidemic individuals contain a cholesteryl ester-rich core that undergoes a thermal transition from a liquid crystalline to an isotropic liquid phase between 20 and 35 °C. LDL from hypertriglyceridemic patients or prepared *in vitro* by the exchange of very low-density lipoprotein for LDL cholesteryl esters is triglyceride-rich, does not have a thermal transition above 0 °C, and exhibits impaired binding to the LDL receptor on normal human skin fibroblasts. Cryoelectron microscopy of LDL quick-frozen from 10 (core-frozen) and 40 °C (core-melted) revealed ellipsoidal particles with internal striations and round particles devoid of striations, respectively. Cryoelectron microscopy of triglyceride-rich LDL prepared *in vitro* revealed particles similar to the core-melted normolipidemic LDL, i.e., round particles without striations. These data suggest that the LDL core in the liquid crystalline phase is characterized by the appearance of striations, whereas LDL with a core that is an isotropic liquid lacks striations. It is suggested that freezing the LDL core into a liquid crystalline phase imposes structural constraints that force LDL from a sphere without partitions to an ellipsoid with partitions. We further suggest that the striation-defined lamellae are a structural feature of a liquid crystalline neutral lipid core that is a determinant of normal binding to the LDL receptor and that conversion of the neutral lipid core of LDL to the isotropic liquid phase via an increase in the temperature or via the addition of triglyceride partially ablates the receptor binding determinants on the LDL surface. This effect is likely achieved through changes in the conformation of apo-B-100. These data suggest that the physical state of the LDL core determines particle shape, surface structure, and metabolic fate.

Plasma concentrations of lipoproteins are risk factors for cardiovascular disease (*1*, *2*). Hypertriglyceridemia occurs in several pathological states, including type 2 diabetes mellitus, where it is associated with other cardiovascular risk factors. These include low plasma concentrations of high-density lipoprotein cholesterol, impaired clearance of postprandial lipemia (*3*), insulin resistance (*4*), increased cholesteryl ester (CE)[1] transfer activity (*5*), and the occurrence of small, dense low-density lipoprotein (LDL) particles (*6*−*9*). Importantly, the triglyceride (TG) content of LDL from hypertriglyceridemic patients is much higher than that of normolipidemic (NL) LDL (*9*, *10*), and the catabolism of small, dense LDL that is rich in TG is distinct from that of NL LDL (*11*).

The association of hypertriglyceridemia with altered LDL composition and catabolism has been linked to differences in its physical and biological properties. The neutral lipid composition of LDL is the major physiological determinant of its structure, thermotropic properties, and binding to the LDL receptor. LDL from HTG patients is TG-rich, and its level of binding to its receptor on human skin fibroblasts is lower than that of NL LDL (*7*−*9*). In addition, TG-rich LDL prepared by *in vitro* exchange of its CE for VLDL-TG also exhibits impaired binding to the LDL receptor. Thus, impaired LDL binding to its receptor is associated with increased TG content and attendant structural changes (*7*−*9*). This effect could also be due to TG-dependent differences in the physical state of the neutral lipid core (*7*, *9*), which as shown by differential scanning calorimetry undergoes a thermal transition at temperatures that decrease as the TG to CE ratio increases (*12*−*17*). Impaired uptake may be due to changes in the core structure or TG-induced changes in the surface structure (*7*−*9*, *18*−*22*) that are associated with atherogenesis (*23*). Thus, it is important to identify differences in hypertriglyceridemic LDL structure that contribute to impaired binding to the LDL receptor.

The structure of LDL has been studied by a number of biophysical methods, including compositional analysis (*24*, *25*), X-ray and neutron scattering (*14*, *26*, *27*), and electron microscopy (*28*−*30*). These studies formed the basis of a model of LDL as a sphere of neutral lipids surrounded by a surface monolayer of proteins and polar lipids. Although electron microscopy of negatively stained particles is a

† This work was supported by grants from the National Institutes of Health to W.C. (RR 02250) and H.J.P. (HL 56865 and HL 30914).

* To whom correspondence should be addressed: MS A-601, Department of Medicine, Baylor College of Medicine, 6565 Fannin St., Houston, TX 77030. Telephone: (713) 798-4160. Fax: (713) 798-5134. E-mail: hpownall@bcm.tmc.edu.

‡ Baylor College of Medicine.

§ Current address: Purdue University, West Lafayette, IN 47907.

‖ University of London.

[1] Abbreviations: CE, cholesteryl ester; LDL, low-density lipoprotein; TG, triglyceride; NL, normolipidemic; HTG, hypertriglyceridemic; VLDL, very low-density lipoprotein; CETP, CE transfer protein; FC, free cholesterol; PL, phospholipid; apo, apolipoprotein.

10.1021/bi0354738 CCC: $25.00
Published on Web 11/21/2003

commonly used technique in the study of lipoprotein morphology (*26*, *28*, *30*, *31*), it has some drawbacks. Conventional electron microscopy of negatively stained LDL particles reveals overall shape and considerable heterogeneity but does not allow imaging of the core because the stain does not penetrate the surface monolayer. Cryoelectron microscopy, on the other hand, provides minimal deformation of the particles within their natural aqueous environment (*32*). Cryoelectron microscopy has been successfully used for studying LDL structure by a number of groups (*33*−*36*). Image analysis of electron cryomicrographs has produced a reconstruction of the three-dimensional structure of LDL, which revealed new features in the structure, a lamellar core organization (*36*). Herein, we show that substitution of TG for CE in LDL is associated with profound structural changes, which can be viewed by cryoelectron microscopy and which may modulate its binding to the LDL receptor and its role in atherogenesis.

EXPERIMENTAL PROCEDURES

LDL was isolated from a single NL donor via flotation at a density (*d*) between 1.019 and 1.063 g/mL. VLDL, from pooled salvaged plasma obtained from The Methodist Hospital Blood Donor Center (Houston, TX), was isolated via flotation at plasma density. TG-rich LDL was prepared by incubating normal LDL with a large excess of VLDL in the presence of the $d > 1.21$ g/mL plasma fraction, which contains CETP activity (*9*, *10*). VLDL (146 mg of TG and 33.4 mg of cholesterol) in 21 mL was combined with 2 mL of LDL (11.6 mg of cholesterol and 1.5 mg of TG), and the volume was reduced to 3 mL with a Centriprep concentrator (Amicon, Beverly, MA). The concentrate was incubated with 3 mL of the $d > 1.21$ g/mL plasma fraction for 8 h at 37 °C, after which its density was adjusted to 1.019 g/mL by adding potassium bromide. Following centrifugation for 18 h (Beckman SW40 rotor at 40 000 rpm), VLDL was removed from the top of the tube by aspiration, by rinsing the upper portion of the tube with distilled water multiple times. The bottom fraction containing TG-rich LDL was then transferred to a test tube and analyzed for TG, CE, free cholesterol (FC), protein, and phospholipid (PL) as well as its electrophoretic mobility on agarose gels. An aliquot of the starting sample of NL LDL was analyzed in the same way.

Lipoprotein compositions were determined on the basis of analyses of TG, FC, CE, and protein concentrations by using commercial kits (Wako). NL and TG-rich LDL were analyzed by agarose gel electrophoresis according to the manufacturer's instructions (Helena Laboratories, Beaumont, TX); lipoprotein mobility was visualized by staining the gels for cholesterol.

Both NL and TG-rich LDL were stored at 4 °C and plunge-frozen over holes on a holey carbon film for cryoelectron microscopy in parallel within 3 days of isolation. The specimens were frozen from 4 to 10 °C and imaged in a JEOL 4000EX cryoelectron microscope at 400 keV as described previously (*36*). The specimens were held at −170 °C in a Gatan 626 cryoholder. The microscope had a Gatan (model 679) 1024 × 1024 slow-scan CCD camera attached directly below the projection chamber and a retractable TV-rate CCD camera (Gatan, model 673) mounted at a 35 mm camera port. Low-dose imaging was carried out using standard techniques described in ref *37*. Cryogrids were searched with a TV-rate CCD camera at a dose rate of 5×10^{-3} electron Å^{-2} s^{-1} in a defocused diffraction mode. Focusing was done off-axis on an area adjacent to a hole selected for imaging at the magnification used for image recording. A 100 μm diameter condenser aperture was used together with a relatively high excitation (spot size 5) of the first condenser lens, resulting in a measured angular source size of 0.15 mrad (*38*). A 50 μm objective lens aperture was used. We used the user function memory slots of the microscope's microprocessor to store and recall settings of lenses and deflection coils for several operational modes, including search, focus, and imaging.

Studies in which NL LDL was frozen from different temperatures were preformed according to the manufacturer's instructions using a computer-controlled vitrification robot (Vitrobot, from Maastricht Instruments Bv, Maastricht, The Netherlands), which reproducibly freezes specimens while controlling sample temperature and humidity prior to freezing. The relative humidity within the Vitrobot chamber was maintained at 80%. Grids (R 2/2, from Quantifoil Micro Tools, Gmbh) were loaded into the chamber. NL LDL (0.1 mL, 0.13 mg of protein/mL) was incubated in buffer for 30 min following equilibration of the internal chamber of the Vitrobot at 10, 30, or 40 °C. LDL (0.004 mL) was applied to grids and robotically blotted (1 s on filter paper) and plunged into liquid ethane cooled with liquid nitrogen. After being frozen, the grids were transferred to liquid nitrogen for storage until they were viewed by cryoelectron microscopy. The vitrified specimens were transferred to a JEOL 1200 electron microscope operated at 100 kV and equipped with a liquid nitrogen-cooled specimen holder (Gatan) for maintaining the specimens in the vitrified state.

Images were collected at a microscope magnification of 40000×. The electron dose used for imaging was 10 electrons/Å^2. Kodak SO-163 photographic films used for imaging were processed for maximum speed and contrast according to the manufacturer's instructions in undiluted Kodak D-19 developer for 12 min at 20 °C. The images were digitized using a SCAI scanner (Zeiss) with a step size corresponding to 3.5 Å on the specimen scale. LDL images were selected interactively in the digitized images and extracted into fields of 120 × 120 pixels. One thousand seven hundred TG-rich LDL particle images were boxed out from 14 micrographs ranging in defocus from 1.5 to 2.2 μm. Defocus values were determined from the positions of contrast transfer function (CTF) zeroes seen in the incoherently averaged spectra of the images from each micrograph (*39*). The data set was processed according to a procedure described previously (*40*).

The images were analyzed with IMAGIC-5 software (*41*). As the first step in image processing, they were aligned and similar particles were grouped into classes using multivariate statistical analysis and classification (*42*, *43*). Images within a class were averaged to enhance the signal-to-noise ratio. The class averages varied in size and appearance. The size appeared to vary incrementally at steps of 30−35 Å.

RESULTS

Low-Density Lipoprotein Composition. Incubation of LDL and VLDL in the presence of the plasma fraction containing

Table 1: Compositions and Diameters of NL LDL, TG-Rich LDL, and Consensus LDL

	composition (% dry mass)[a]							
	core lipids		surface components				diameter (Å)	
LDL	TG	CE	FC	PL	protein	TG:CE	particle	core
NL	5.9	37.1	8.8	22.2	26.0	0.16	186	145
TG-rich	23.8	26.7	7.1	21.6	20.7	0.89	191	154
consensus	6.0	42.0	8.0	22.0	22.0	0.14	198	159

[a] Consensus composition data from Havel and Kane (*44*).

CETP altered the lipoprotein composition. The major compositional change was in the relative amounts of CE and TG (Table 1). NL LDL is similar in composition to its reported (*44*) consensus values. There were small differences in the relative amounts of FC, PL, and protein in NL LDL and TG-rich LDL. In contrast, TG-rich LDL contained more TG and less CE than NL LDL, so the ratio of TG to CE was increased from 1:6 to 1:1. The latter ratio corresponds to a composition range in which the binding of LDL to its receptor on fibroblasts is impaired and a thermal transition in the core is not detectable (*9*).

LDL size was calculated from the partial specific volumes of each of the components as reported by Tardieu et al. (*45*) and their respective molar ratios relative to apolipoprotein (apo) B-100, which is assumed to have a partial specific volume of 0.73 mL/g and to occur in LDL at only one copy per particle. In our calculations, we used the following molecular weights (molecular volumes): 387 (642 Å^3) for FC, 647 (1133 Å^3) for CE, 858 (1586 Å^3) for TG, 770 (1253 Å^3) for PL, and 550 000 (669 000 Å^3) for apo-B-100. The calculated particle volumes (V_P, cubic angstroms) are given by the equation $V_P = 669 + [963(CE) + 1017(TG) + 912(FC) + 940(PL)]/(apo\text{-}B\text{-}100)$, where CE, TG, FC, PL, and apo-B-100 are concentrations expressed as weight of analyte per unit volume, typically milligrams per milliliter. The calculated volumes of the neutral lipid core (V_C) were obtained from the equation $V_C = [963(CE) + 1017(TG)]/(apo\text{-}B\text{-}100)$. The corresponding core and particle diameters are given by the relationship $D = 2(3V/4\pi)^{1/3}$. The calculated diameters for NL LDL and TG-rich LDL particles are 186 and 191 Å, respectively; the corresponding diameters of the neutral lipid core (CE and TG) are 145 and 154 Å, respectively (Table 1). The calculated dimensions of NL LDL are similar to those based on the consensus data of Havel and Kane (*44*). The calculated diameters for LDL correspond favorably with the reported dimensions (*36*) of 250 Å × 205 Å × 180 Å (mean diameter of 212 Å). The difference may be due in part to contributions of water to the volumes observed with the frozen hydrated specimens in the cryoelectron microscope; the dimensions calculated from LDL composition do not include water.

Low-Density Lipoprotein Electrophoretic Mobility. The electrophoretic mobilities of NL LDL and TG-rich LDL were different as well (Figure 1). The peak for NL LDL cholesterol was symmetrical and exhibited the expected β mobility. In contrast, the peak for TG-rich LDL cholesterol was shifted toward pre-β mobility and appeared between β and pre-β mobility, a change that corresponds to a negative charge that is greater than that of NL LDL.

Cryoelectron Microscopy of Low-Density Lipoproteins. According to previous studies of the thermotropic properties

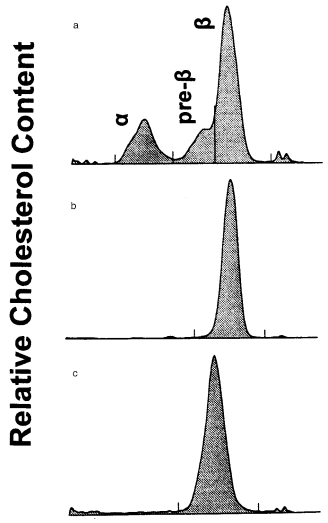

FIGURE 1: Results of agarose gel electrophoresis: (a) NL plasma (from left to right, mobilities are α, pre-β, and β), (b) NL LDL, and (c) TG-rich LDL.

of NL LDL, the core is melted at or above 40 °C and frozen at 10 °C, with the transition temperature from the core-frozen to core-melted state appearing between 20 and 35 °C (*9*, *46*). To identify distinct structures that might be associated with core-frozen and core-melted LDL, image fields of NL LDL frozen from 10 and 40 °C, respectively, were collected. As shown in Figure 2, the LDL particles have profoundly different structures at 10 and 40 °C. Core-frozen LDL is characterized by an ellipsoidal morphology containing numerous striations as previously described by Orlova et al. (*36*; Figure 2a). In contrast, most core-melted LDL particles are round and devoid of striations (Figure 2c). At 30 °C, a mixture of ellipsoidal, striated particles and round, nonstriated particles was observed (Figure 2b).

A representative cryoelectron microscopy image field containing TG-rich LDL is shown in Figure 3a. In contrast to NL LDL, TG-rich LDL was heterogeneous and appeared largely as round, core-melted particles that were grossly similar to the structures of NL LDL in Figure 2 and reported by Orlova et al. (*36*); a representative image field of the latter appears as Figure 3b. TG-rich and NL LDL particles had nearly the same diameters (see also Table 1). Whereas the NL LDL particles were striated when ellipsoidal and nonstriated when more round, the great majority of TG-rich LDL particles were nonstriated.

The signal-to-noise ratios of the cryoelectron microscopy images of individual LDL particles, which were taken under low-dose conditions, were not suitable for additional analysis. To improve the signal-to-noise ratio, we averaged similar particle images by using a multivariate statistical approach (*41*). Similar particles were sorted into classes, which were averaged to obtain better representations of particle views in different directions while the noise present in the original images was suppressed. All 1700 boxed-out TG-rich LDL particles were grouped into 100 classes, with 10−20 particles per class. Some class average images are shown in Figure 4. The class average TG-rich LDL particles were similar in size and shape to normal LDL (*36*) but lacked the striations that in our previous study characterized NL LDL projections in some directions. Notably, only two classes of TG-rich LDL, together comprising 20 particles (<2% of the boxed-

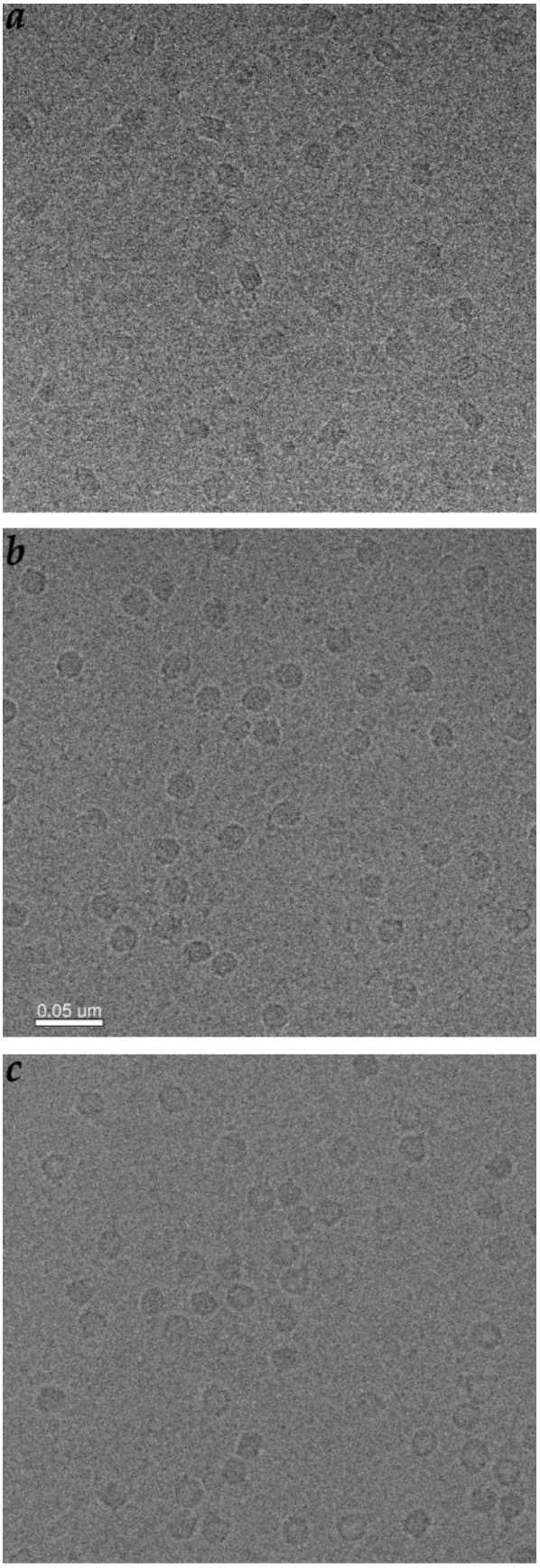

FIGURE 2: Electron images (400 keV) of general fields of NL LDL particles embedded in vitreous ice after rapid freezing from (a) 10, (b) 30, and (c) 40 °C.

out TG-rich LDL particles), contained particles with striations; the remainder (~98%) did not contain striations.

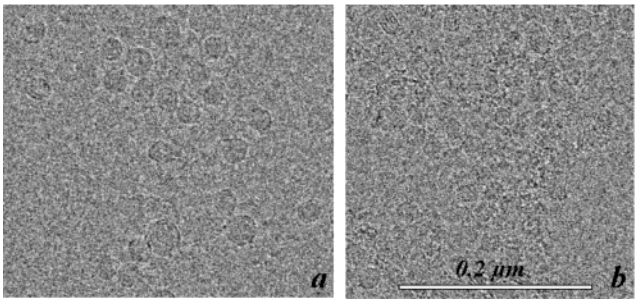

FIGURE 3: Electron images (400 keV) of general fields of LDL particles embedded in vitreous ice: (a) TG-rich LDL and (b) NL LDL. Both groups of LDL particles are equally heterogeneous and grossly similar. The bar is 0.2 μm. The NL LDL in panel b is the same LDL preparation used to make TG-rich LDL shown in panel a.

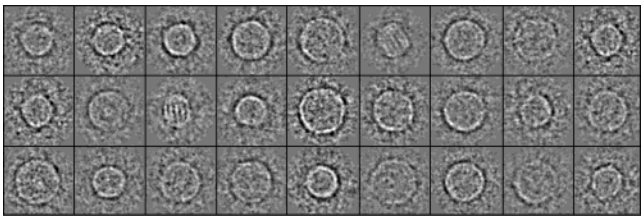

FIGURE 4: Selected class average images of TG-rich LDL particles. The preponderance of TG-rich particles did not have striations. At the same time, the parallel control preparation of normal LDL did display them. The overall shape and dimensions of TG-rich LDL are similar to that of normal LDL. Two classes (row 1, column 6, and row 2, column 3) that exhibited striations and a more ellipsoidal shape than the remainder of the particles represented less than 2% of the total number of particles. The boxes are 420 Å on each side.

The occurrence of such a small proportion of striated TG-rich LDL particles likely represents incomplete TG enrichment of all LDL particles. Because the NL and TG-rich LDL particles prepared in parallel were similar in size and shape, it is likely that they would be similar in angular distribution. An absence of striations in TG-rich LDL would suggest an absence of the lamellar core that characterizes NL LDL.

DISCUSSION

Compared to NL LDL, LDLs from hypertriglyceridemic patients are smaller, denser, and TG-rich and have a conformationally distinct apo-B-100 (*7*−*9*). Because small, dense LDL is TG-rich, one might expect its core structure to differ from that of NL LDL. A model of LDL, developed from low-angle X-ray and neutron scattering studies, consists of a neutral lipid core surrounded by a monolayer of protein and polar lipids (*45*, *46*, *48*). The model is consistent with the very low solubilities of CE and TG and the amphiphilic character of the PL and protein. The CE-rich core of LDL undergoes a thermal transition from a liquid crystalline to an isotropic liquid phase; the transition temperature of LDL decreases when the TG content of LDL increases (*12*−*17*, *49*). Pregetter et al. (*16*) proposed a model of LDL comprising a highly fluid, TG-rich central core surrounded by a CE-rich shell that undergoes a phase transition. Although that model accommodates most of our current knowledge of LDL, it was based on one-dimensional X-ray scattering data. In contrast, the structure of human NL LDL below its phase transition, obtained by three-dimensional reconstruction of electron microscopic images of particles embedded in

vitreous ice, revealed a nonspherical, higher-density outer shell and a lower-density inner lamella-like core (*36*).

Previous studies (*9*, *46*) have shown that the physical state of the core lipids of LDL is a function of composition and temperature. NL LDL exhibits a broad thermal transition from a liquid crystalline to an isotropic liquid phase that peaks between 20 and 35 °C; thus, above 40 °C nearly all core lipids are isotropic liquids, and below 10 °C, the core is largely liquid crystalline. Our data show for the first time that temperature is a profound determinant of LDL core morphology such that distinct structures are observed above and below the putative transition temperature for the melting of LDL core lipids. At 10 °C, LDL is core-frozen and has an ellipsoidal morphology containing striations within the core. At 40 °C, LDL is core-melted and grossly round but lacks the striations characteristic of core-frozen LDL.

Addition of TG to LDL lowers its transition temperature, and at very high TG-to-CE ratios, a thermal transition is not observed above 0 °C, the practical lower limit for differential scanning calorimetry of aqueous samples (*9*, *46*). Thus, TG-rich LDLs are expected to have an isotropic liquid core at temperatures above 0 °C. In the study presented here, NL LDL and TG-rich LDL, which were isolated and analyzed in parallel, differed both macro- and microscopically. They exhibited different electrophoretic mobilities; the TG-rich LDL peak was closer to pre-β mobility. Cryoelectron microscopy shows that on a microscopic scale TG-rich LDL particles are grossly similar in size to NL LDL but do not exhibit the striations that Orlova et al. (*36*) reported for NL LDL. Moreover, relative to NL LDL, the TG-rich LDL has a preponderance of particles that are round rather than ellipsoidal. Thus, the morphology of TG-rich LDL is similar to that of core-melted NL LDL (Figure 2c).

LDLs are grossly round particles that are heterogeneous with respect to size, density, and composition (*26*−*30*, *33*−*35*, *50*, *51*). Our previous study (*36*) showed that particles have discrete variations in size and suggested that LDLs can have discrete structures. Unlike our TG-rich LDL, the NL LDL always exhibited striations in certain orientations regardless of the size, suggestive of a distinct core that is frozen. The TG-rich LDLs used in the current study were formed from NL LDL *in vitro* using CETP and TG-rich native VLDL particles (*10*). TG-rich LDLs are similar to native small, dense LDLs from hypertriglyceridemic patients with respect to electrophoretic mobility, the physical state of the core, protein content, and receptor binding (*9*). However, *in vitro* TG-rich LDL is larger than native, small, dense LDL because the TGs that replace the CE in the CETP-mediated exchange reaction have a larger partial specific volume (Table 1). This difference could explain some differences between the shapes of particles we observed and the discoidal particles recently reported for small, dense LDL (*34*).

NL LDL has a high affinity for its receptor on normal human skin fibroblasts (*7*−*9*). NL LDLs, frozen from 10 °C, are CE-rich and core-frozen, and exhibit striations in cryoelectron microscopic images with a preponderance of ellipsoidal particles (*9*, *36*). When cooled from 40 °C, the LDLs are core-melted and show no striations within nearly spherical particles (*9*, *36*). In contrast, TG-rich LDL exhibits impaired binding to LDL receptors on human skin fibroblasts (*7*−*9*). Like core-melted NL LDL, TG-rich LDL, which does not exhibit a detectable thermal transition (*9*), exhibits virtually no striations in its cryoelectron microscopic images and contains a preponderance of round particles. Our findings support the hypothesis that the lamellae in the core of NL LDL originate from liquid crystalline CE. From these data, we believe that the physical state of LDL as defined by the lamellar structure is an important determinant of LDL binding to the LDL receptor. The role of the lamellae in that binding is probably indirect, because the core is shielded by the surface monolayer of the PL and protein and is not likely to be accessible to the LDL receptor. A more likely scenario is that lipid−lipid and lipid−protein interactions between the core and surface, which contains apo-B-100 and polar lipids, alter the surface structure and the recognition and binding of LDL (*7*−*9*). This is consistent with our previously reported data (*9*), which showed that apo-B-100 differs in structure between TG-rich LDL and NL LDL. Studies of other lipoproteins, such as β-LDL from rabbits or swine fed an atherogenic diet (*15*, *22*), should reveal whether the striations within the lipoprotein core are characteristic of CE-rich lipoproteins.

REFERENCES

1. Gotto, A. M., Jr., and Pownall, H. J. (2003) *Manual of Lipid Disorders: Reducing the Risk for Coronary Heart Disease*, 3rd ed., Lippincott, Williams and Wilkins, Baltimore.
2. Hobbs, H. H., Russell, D. W., Brown, M. S., and Goldstein, J. L. (1990) *Annu. Rev. Genet. 24*, 133−170.
3. Georgopoulos, A., and Phair, R. D. (1991) *J. Lipid Res. 32*, 1133−1141.
4. Reaven, G. M. (1995) *Physiol. Rev. 75*, 473−486.
5. Bagdade, J. D., Ritter, M. C., and Subbaiah, P. V. (1991) *J. Clin. Invest. 87*, 1259−1265.
6. Gray, R. S., Robbins, D. C., Wang, W., Yeh, J. L., Fabsitz, R. R., Cowan, L. D., Welty, T. K., Lee, E. T., Krauss, R. M., and Howard, B. V. (1997) *Arterioscler. Thromb. Vasc. Biol. 17*, 2713−2720.
7. Aviram, M., Lund-Katz, S., Phillips, M. C., and Chait, A. (1988) *J. Biol. Chem. 263*, 16842−16848.
8. Kleinman, Y., Eisenberg, S., Oschry, Y., Gavish, D., Stein, O., and Stein, Y. (1985) *J. Clin. Invest. 75*, 1796−1803.
9. McKeone, B. J., Patsch, J. R., and Pownall, H. J. (1993) *J. Clin. Invest. 91*, 1926−1933.
10. Pownall, H. J., Brauchi, D., Kilinc, C., Osmundsen, K., Pao, Q., Payton-Ross, C., Gotto, A. M. J., and Ballantyne, C. M. (1999) *Atherosclerosis 143*, 285−297.
11. Vega, G. L., and Grundy, S. M. (1989) *J. Intern. Med. 226*, 5−15.
12. Deckelbaum, R. J., Shipley, G. G., Small, D. M., Lees, R. S., and George, P. K. (1975) *Science 190*, 392−394.
13. Deckelbaum, R. J., Tall, A. R., and Small, D. M. (1977) *J. Lipid Res. 18*, 164−168.
14. Laggner, P., Degovics, G., Muller, K. W., Glatter, O., Kratky, O., Kostner, G., and Holasek, A. (1977) *Hoppe-Seyler's Z. Physiol. Chem. 358*, 771−778.
15. Pownall, H. J., Jackson, R. L., Roth, R. I., Gotto, A. M., Patsch, J. R., and Kummerow, F. A. (1980) *J. Lipid Res. 21*, 1108−1115.
16. Pregetter, M., Prassl, R., Schuster, B., Kriechbaum, M., Nigon, F., Chapman, J., and Laggner, P. (1999) *J. Biol. Chem. 274*, 1334−1341.
17. Tall, A. R., Atkinson, D., Small, D. M., and Mahley, R. W. (1977) *J. Biol. Chem. 252*, 7288−7293.
18. Mims, M. P., Chari, M. V., and Morrisett, J. D. (1986) *Biochemistry 25*, 7494−7501.
19. Mims, M. P., Guyton, J. R., and Morrisett, J. D. (1986) *Biochemistry 25*, 474−483.
20. Mims, M. P., and Morrisett, J. D. (1988) *Biochemistry 27*, 5290−5295.
21. Mims, M. P., Soma, M. R., and Morrisett, J. D. (1990) *Biochemistry 29*, 6639−6647.
22. Morrisett, J. D., Gaubatz, J. W., Tarver, A. P., Allen, J. K., Pownall, H. J., Laggner, P., and Hamilton, J. A. (1984) *Biochemistry 23*, 5343−5352.

23. Fraser, R., Vesselinovitch, D., and Wissler, R. W. (1976) *Pathology 8*, 57−68.
24. Edelstein, C., Kezdy, F. J., Scanu, A. M., and Shen, B. W. (1979) *J. Lipid Res. 20*, 143−153.
25. Shen, B. W., Scanu, A. M., and Kezdy, F. J. (1977) *Proc. Natl. Acad. Sci. U.S.A. 74*, 837−841.
26. Luzzati, V., Tardieu, A., and Aggerbeck, L. P. (1979) *J. Mol. Biol. 131*, 435−473.
27. Laggner, P., and Müller, K. W. (1978) *Q. Rev. Biophys. 11*, 371−425.
28. Chatterton, J. E., Phillips, M. L., Curtiss, L. K., Milne, R., Fruchart, J.-C., and Schumaker, V. N. (1995) *J. Lipid Res. 36*, 2027−2037.
29. Lund-Katz, S., and Phillips, M. C. (1986) *Biochemistry 25*, 1562−1568.
30. Gulik-Krzywicki, T., Yates, M., and Aggerbeck, L. P. (1979) *J. Mol. Biol. 131*, 475−484.
31. Chatterton, J. E., Phillips, M. L., Curtiss, L. K., Milne, R. W., Marcel, Y. L., and Schumaker, V. N. (1991) *J. Biol. Chem. 266*, 5955−5962.
32. Dubochet, J., Adrian, M., Chang, J. J., Homo, J. C., Lepault, J., McDowall, A. W., and Schultz, P. (1988) *Q. Rev. Biophys. 21*, 129−228.
33. Spin, J. M., and Atkinson, D. (1995) *Biophys. J. 68*, 2115−2123.
34. Antwerpen, R. V., and Gilkey, J. C. (1994) *J. Lipid Res. 35*, 2223−2231.
35. van Antwerpen, R., Chen, G. C., Pullinger, C. R., Kane, J. P., LaBelle, M., Krauss, R. M., Luna-Chavez, C., Forte, T. M., and Gilkey, J. C. (1997) *J. Lipid Res. 38*, 659−669.
36. Orlova, E. V., Sherman, M. B., Chiu, W., Mowri, H., Smith, L. C., and Gotto, A. M. (1999) *Proc. Natl. Acad. Sci. U.S.A. 96*, 8420−8425.
37. Sherman, M. B., Brink, J., and Chiu, W. (1996) *Micron 27*, 129−139.
38. Spence, J. C. H. (1988) *Experimental high-resolution electron microscopy*, 2nd ed., Oxford University Press, New York.
39. Zhou, Z. H., Hardt, S., Wang, B., Sherman, M. B., Jakana, J., and Chiu, W. (1996) *J. Struct. Biol. 116*, 216−222.
40. Serysheva, I. I., Orlova, E. V., Chiu, W., Sherman, M. B., Hamilton, S. L., and van Heel, M. (1995) *Nat. Struct. Biol. 2*, 18−24.
41. van Heel, M., Harauz, G., and Orlova, E. V. (1996) *J. Struct. Biol. 116*, 17−24.
42. van Heel, M., and Frank, J. (1981) *Ultramicroscopy 6*, 187−194.
43. Frank, J. (1995) *Three-dimensional electron microscopy of macromolecular assemblies*, Academic Press, New York.
44. Havel, R. J., and Kane, J. P. (2001) in *The Metabolic and Molecular Bases of Inherited Disease* (Scriver, C. R., Beaudet, A. L., Sly, W. S., and Valle, D., Eds.) pp 2705−2716, McGraw-Hill, New York.
45. Tardieu, A., Mateu, L., Sardet, C., Weiss, B., Luzzati, V., Aggerbeck, L., and Scanu, A. M. (1976) *J. Mol. Biol. 105*, 459−460.
46. Deckelbaum, R. J., Shipley, G. G., and Small, D. M. (1977) *J. Biol. Chem. 252*, 744−754.
47. Atkinson, D., Deckelbaum, R. J., Small, D. M., and Shipley, G. G. (1977) *Proc. Natl. Acad. Sci. U.S.A. 74*, 1042−1046.
48. Muller, K., Laggner, P., Glatter, O., and Kostner, G. (1978) *Eur. J. Biochem. 82*, 73−90.
49. Sklar, L. A., Craig, I. F., and Pownall, H. J. (1981) *J. Biol. Chem. 256*, 4286−4292.
50. Laggner, P. (1976) in *Low-density lipoproteins* (Day, C. E., and Levy, R. S., Eds.) pp 49−69, Plenum Press, New York.
51. Myant, N. B. (1990) *Cholesterol metabolism, LDL, and the LDL receptor*, Academic Press, New York.

BI0354738